73rd International Astronautical Congress (IAC), Paris, France, 18-22 September 2022.

IAC-22,B4,4,x74115

Comparing pre- and post-launch images from the HYPSO-1 cubesat hyperspectral imager

Marie Bøe Henriksen[a,b*], Joseph L. Garrett[a], Tor Arne Johansen[a], Fred Sigernes[b]

[a]*Department of Engineering Cybernetics, Center for Autonomous Marine Operations and Systems, Norwegian University of Science and Technology, 7034 Trondheim, Norway, *marie.b.henriksen@ntnu.no*
[b]*Department of Arctic Geophysics, University Center in Svalbard, 9171 Longyearbyen, Norway*

Abstract

HYPSO-1, a 6U cubesat carrying a hyperspectral imaging payload for ocean color observation, was launched in January 2022. During the commissioning and validation phases, the satellite and payload performance were tested. The hyperspectral imager, a visible to near infrared pushbroom instrument based on a transmissive grating design and built out of commercial off-the-shelf components, was thoroughly calibrated and characterized prior to launch. During launch, however, the satellite and payload endured strong forces, and tiny movements or changes to the components, particularly the components in the optical train of the hyperspectral imager, can affect the resulting data products. Pre-launch testing showed that sub-millimeter shifts of optics spacing and component orientation resulted in measurable performance degradation. Careful on-orbit calibration and validation is therefore important to understand the data and its limitations. Here we present the observed changes in the recorded raw spectrograms between data gathered during the pre-launch calibration campaign and data from the post-launch validation campaign. Most noticeable is a spatial shift of 7 pixels, most likely due to movement of the slit, and a smudge appearing on the spectrograms at about 500 nm. In addition, an example of correction by destriping is shown to account for the spatial shift.

Keywords: Hyperspectral imaging, Cubesat, Post-launch instrument performance.

Acronyms/Abbreviations

AOI	Area of Interest
COTS	Commercial Off-the-Shelf
EM	Engineering Model
FM	Flight Model
FWHM	Full Width at Half Maximum
HAB	Harmful Algae Bloom
HSI	Hyperspectral Imager
HYPSO	HYPerspectral Smallsat for ocean Observation
NIR	Near Infrared
NTNU	Norwegian University of Science and Technology
QM	Qualification Model
RMSE	Root Mean Square Error
RTS	Random Telegraph Signal
SNR	Signal-to-Noise Ratio
TVAC	Thermal-Vacuum
VIS	Visible

1. Introduction

The HYPerspectral Smallsat for ocean Observation (HYPSO) mission is a mission from the Norwegian University of Science and Technology (NTNU) that aims to collect oceanographic observations in support of marine research. The main goal is to detect, map and investigate ocean color phenomena such as algae blooms, including Harmful Algae Blooms (HABs), using a Hyperspectral Imager (HSI). The first satellite, HYPSO-1, is a 6U cubesat that was launched January 13 2022 into a 540 km Sun-synchronous orbit, with mission parameters presented in greater detail in [1]. It will be followed by a second cubesat, HYPSO-2, that is planned to be launch in 2024 with a similar payload.

The main payload is a pushbroom HSI, which is further described in Section 2. It is a pushbroom imager which covers the Visible (VIS) to Near Infrared (NIR) spectral range with a spectral resolution of about 5 nm. The spectral signatures observed by the HSI will be used to recognize algae blooms in the ocean.

Prior to launch, the hyperspectral payload was thoroughly calibrated and characterized, as described in [2]. During pre-launch testing, the spectral and spatial focus of the instrument was observed to be easily affected by sub-millimeter shifts of components in the optical train. This indicates that small movements from launch could affect the optical performance.

Pre-launch testing was performed on an Engineering Model (EM) and a Qualification Model (QM), which are close to identical models of the Flight Model (FM) that is flown on the satellite. The EM and QM were used for testing on ground to minimize stress on the FM. These tests include shock, vibration, radiation, thermal, vacuum and Thermal-Vacuum (TVAC) tests, and are described in [3]. During thermal and TVAC tests, a spectral shift was observed, which was further investigated in [4]. Both small

Table 1. Specifications of the hyperspectral imager.

Parameter	Specification
Sensor	Sony IMX249
Image size	(1936, 1216) pixels
Area of interest[1]	pixel (428:1508, 266:950)
Bit depth	12-bit
Spectral range	400 - 800 nm
Grating	300 grooves/mm
Slit dimensions	7 mm x 50 μm
Theoretical FWHM	3.33 nm
Measured FWHM	3.85 nm

[1]Pre-selected AOI, can be changed if needed.

Table 2. Specifications of the hyperspectral imager.

Dataset	Dates(s)	Description
0a	2022-03-18	Dark frame (pre-launch)
0b	2022-03-18	Radiometric calibration frame (pre-launch)
1a-1	2022-06-20	Dark cube, pointing up[1]
1a-2	2022-06-20	Dark cube, pointing up
1b-1	2022-05-14	Dark cube, pointing down[2]
1b-2	2022-06-23	Dark cube, pointing down
1b-3	2022-05-04	Dark cube, pointing down
2a	2022-02-01	Sahara cube
2b	2022-02-01	Sahara frame
3a	2022-08-06	Sørøya cube

[1]Pointing up towards outer space
[2]Pointing down towards dark ocean

spectral shifts and change of imaging focus with temperature were recorded. These effects might be present in the HYPSO-1 instrument after launch too, motivating the need for the instrument being characterized and monitored using post-launch data.

After launch, time was spent on commissioning, testing and validation of the satellite and hyperspectral payload. This paper presents some of the initial characterization of the hyperspectral imager performance after launch. The findings are compared to the pre-launch calibration data, and changes from the pre- to post-launch data discussed. In addition, an simple algorithm for destriping hyperspectral images shows an example of how additional in-flight sensor validation could be used to facilitate the analysis of collected images.

2. Hyperspectral instrument

The hyperspectral instrument onboard HYPSO-1 is a pushbroom HSI in the VIS-NIR range. It is based on a transmissive grating design with Commercial Off-the-Shelf (COTS) components as presented in [5], with modifications for the space environment as described in [6]. The Area of Interest (AOI) (on the sensor) covers a spectral range from 400 nm to 800 nm, and the measured Full Width at Half Maximum (FWHM) is less than 4.5 nm for all wavelengths. More information on the instrument characteristics prior to launch can be found in [2]. From a 500 km orbit, the swath width covers 40 km with the selected AOI, and a spatial resolution of around 100 m is expected. A summary of the instrument specifications is shown in Table 1.

Each frame recorded at the sensor is as a spectrogram. Focused light from the front lens enters a slit, so that a 1-spatial-dimensional image is captured at the time. A grating disperses the light so that different wavelengths of light are recorded at different horizontal positions along the sensor. The spectrogram therefore records spatial information along the y-axis, and wavelength along the x-axis. In the pushbroom configuration, one spectrogram is captured at a time with a moving imager (or moving target), so that the images can be stitched together to form a hyperspectral data cube. The cube then has a 2-spatial-dimensional image of the area covered by the instrument, with a third dimension holding spectral information for each pixel.

3. Datasets

An overview of the datasets that are used is shown in Table 2. Dataset 0 is from pre-launch calibration, dataset 1 is dark data collected by HYPSO-1 in-orbit both pointing up towards outer space and down towards the dark oceans. Dataset 2 is captured from above the Sahara desert, while dataset 3 is captured above the island Sørøya in Finnmark, Norway. Datasets containing a frame denotes that only one frame/spectrogram is used, while a cube means that the full hyperspectral cube is used in the analysis.

The HYPSO-1 datasets either consist of full frames or a binned hyperspectral cube. A full frame is what is recorded by the sensor at maximum pixel resolution. The standard data product is a hyperspectral cube that only includes pixels within the AOI, and spectrally bins the data a factor of 9 (full frame cubes and/or no binning can also be captured upon request). The standard data cube consists of 965 frames.

4. Data analysis

The analysis is performed on raw data. The only calibration applied is spectral calibration, which assigns a wavelength to each pixel. Radiometric calibration and other corrections, such as smile and keystone correction, are not applied, except for in Section 4.5.

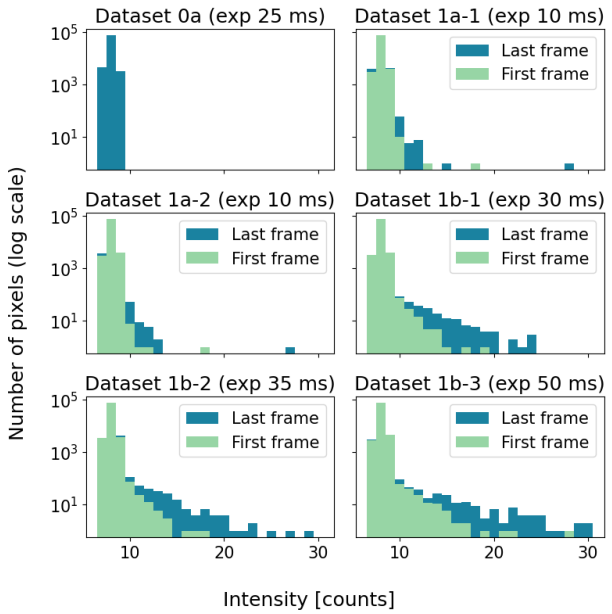

Fig. 1. Distribution of recorded values in dark datasets. The datasets are described in Table 2.

Table 3. Hot pixels counted in dark datasets. Case 1 is all hot pixels counted in any frame in the cube, case 2 is all hot pixels counted in more than half of the frames in the cube, and case 3 is all the hot pixels counted in every frame in the cube. The datasets are described in Table 2.

Dataset	**Case 1: (any frame) # hot pixels**	**Case 2: (1/2 frames) # hot pixels**	**Case 3: (all frames) # hot pixels**
0a	0	-	-
1a-1	2	1	1
1a-2	4	3	1
1b-1	46	18	2
1b-2	41	17	2
1b-3	98	45	6
All	0	0	0

4.1 Dark images

Dark signal, here also referred as background values, is the signal recorded by the sensor when no light is present, and is caused by thermally generated electrons collected by the sensor. Shifts in the mean dark signal can lead to systematic errors if not accounted for, and depends on the residence time of the signals in the sensor, in addition to increasing with increasing temperature [7].

Several dark data cubes have been captured by HYPSO-1, both pointing up towards outer space and down towards the ocean during night time. Different exposure times have been used, as different exposure times are often used for observations. Other camera settings such as frames per second, number of frames etc. have been kept constant. The dark cubes captured only cover the AOI and are spectrally binned. For the comparison with dark pre-launch calibration data, the dark frame was also cropped to AOI and spectrally binned prior to the analysis. To investigate dark signal in the datasets, a histogram showing the distribution of pixel values in the frame is plotted, seen in Figure 1. For the pre-launch dark calibration frame (dataset 0a), only 1 frame was used, while for the data cubes the first and last frames (frame 0 and frame 955) in the cube are plotted.

During a capture, power is consumed and heat is generated and released. Logs show that the temperature typically increases from 16 to 22 degrees Celsius while capturing a hyperspectral data cube with exposure time of 30 ms. It can be seen in Figure 1 that the last frame contains higher maximum values, and a larger amount of higher values than the first frame for all data cubes. This is consistent with background values increasing with increasing temperature. In addition, it can be noted that the data cubes with longer exposure times show higher values in both the first and last frames, suggesting that the mean dark signal also increases with exposure time.

4.1.1 Hot pixels

Hot pixels are pixels that record higher values than what is expected from the incoming light. An investigation of hot pixels in the HYPSO-1 data was done using the dark data cubes. A pixel value of two times the average value in the first frame was used as a threshold, and all pixels with values above this threshold counted as hot pixels. Hot pixels were marked in every frame in the data cube, and the number of hot pixels counted are shown in Table 3. Case 1 is the number of pixels in the cube that registered a hot pixel value in any frame, case 2 is the number of pixels that registered a hot pixel value in more than half of the frames in the cube, while case 3 is the number of pixels that registered a hot pixel value in all frames in the cube. Since only one frame was used from the pre-launch calibrated data, it is only shown for case 1. In addition, the pixel location of the hot pixels were marked so that they could be compared between different datasets. As seen in the table, no pixels recorded hot pixel values in all of the data cubes.

The results in Table 3 suggest that number of hot pixels increases with temperature and exposure time, and that some hot pixels are random while others last for the whole capture, but that they are all reset between each capture. That there are more hot pixels appearing for half of the frames than for all the frames in the cube suggests that some of the hot pixel values are not constant, but randomly jumping, known as Random Telegraph Signals (RTSs) [7]. That the hot pixels are not consistent and

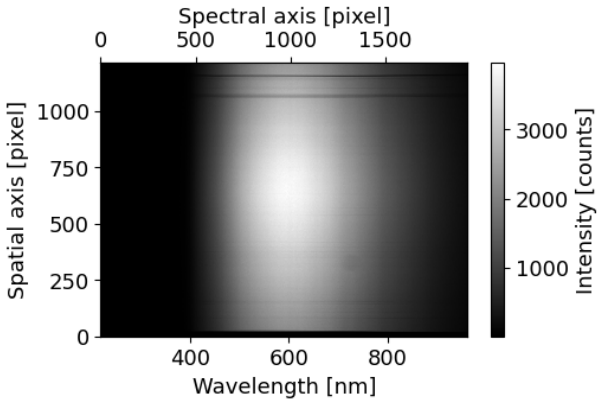

Fig. 2. Radiometric calibration frame (dataset 0b).

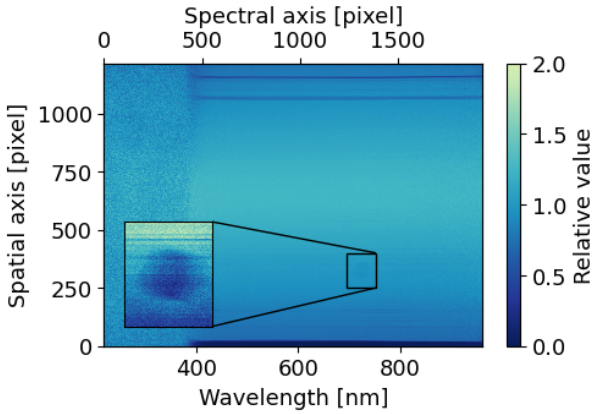

Fig. 3. Relative response of radiometric calibration frame. Smudge marked at spatial pixels 250:400 and spectral pixels 1240:1390.

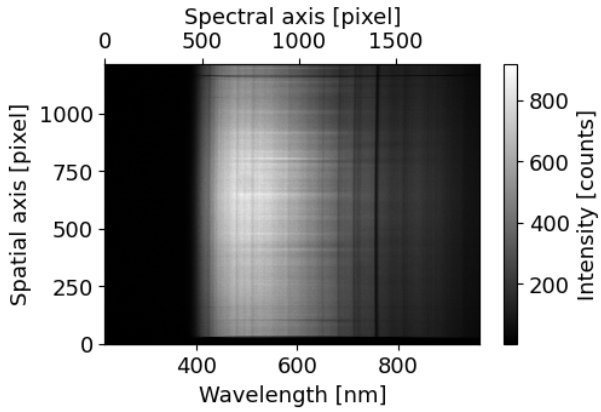

Fig. 4. Sahara frame (dataset 2b).

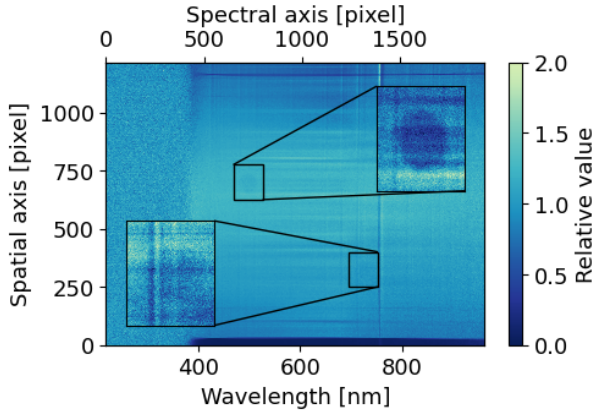

Fig. 5. Relative response of Sahara frame. The first smudge marked at spatial pixels 250:400 and spectral pixels 1240:1390, and the second smudge spatial pixels 625:775 and spectral pixels 650:800.

recorded in the same location every time makes it harder to correct pixels with a hot pixel mask or similar, since a new mask would have to be created for each capture.

4.2 Spectrogram artifacts

Some artifacts, such as blobs/smudges and dust stripes were observed in the spectrogram before launch, as seen in Figure 2 which shows a spectrogram from radiometric calibration in the lab. Vignetting is visible at the edges, as reported in [2], however, two dust stripes can also be seen in the top of the image at spatial pixel 1050 and 1140. In addition, a small smudge can be seen at spatial pixel 300 and spectral pixel 1300 (wavelength 720 nm). This smudge is more prominent in Figure 3 which shows the relative response of the calibration frame, zooming in on the location with the smudge in the box. The relative response is calculated by dividing the full frame by the absolute response, where the absolute response is the average signal per wavelength (average row in the frame), as described in [2]. In the bottom of the image, a darker edge can be seen, which marks the lower edge of the slit. The slit is not centered perfectly, which results in the lower edge being visible in the spectrogram.

The Sahara Desert is imaged to provide nearly uniform illumination so that a spectrogram can be compared to the ground calibration. Figure 4 shows a full frame spectrogram of the Sahara Desert, captured by HYPSO-1 in-orbit. The surface of the desert is quite bright and uniform. However, as it is not perfectly uniform, some features are present. This makes the signal vary slightly across the slit, which appears as horizontal features in the spectrogram. Atmospheric features, which are also visible in the data, cause absorption lines which can be seen as vertical stripes in the frame.

Overall, the intensity in the image is lower in the Sahara image than in the pre-launch calibration image, giving lower Signal-to-Noise Ratio (SNR), meaning that noise might be more apparent in the data. One horizontal dust stripe is visible at spatial pixel 1150, while the second stripe seen in the calibration data is not as apparent. Either it has disappeared, or it might be mixed with

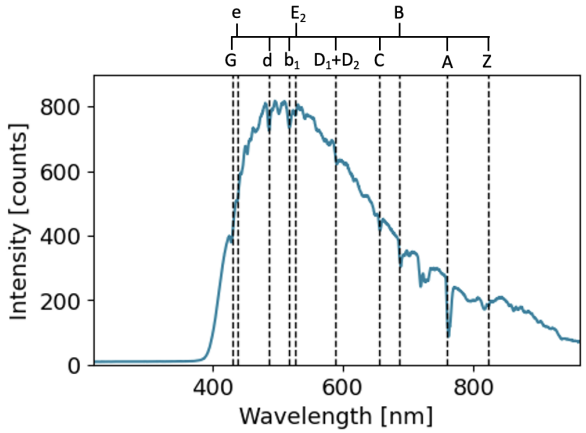

Fig. 6. Sahara frame (dataset 2b), center row, with Fraunhofer lines marked (dashed black lines).

the features seen across the slit. A smudge appears, but this time around spatial pixel 700 and spectral pixel 700 (wavelength 500 nm). The first smudge seen in the calibration data is not as distinguishable in the Sahara frame. This might be due to the lower light level, so that the smudge feature disappears in the noise, or it might no longer be present. Zoomed in boxes on both locations are marked in Figure 5, which shows the relative response of the Sahara frame.

4.3 Spectral shift

During pre-launch calibration, spectral calibration coefficients are found to determine the wavelength corresponding to each pixel element on the sensor. Since the payload must endure strong forces during launch, and small movements of components can affect the optical path, any spectral shift after launch should be reported.

Fraunhofer lines are known absorption lines from the Sun spectrum. Since these absorption lines appear at known wavelengths, they can be used to assess the spectral calibration post launch, and detect potential spectral shifts in the spectrogram. A spectral shift can also be estimated by monitoring the oxygen A-band, with center wavelength around 760 nm [8, 9]. To determine the shift post launch, the difference of the center position of the band is calculated. When comparing with pre-launch data, however, the wavelength location must be used, since HYPSO-1 did not acquire any data with atmospheric absorption lines prior to launch.

The Sahara frame (dataset 2b) is again used to investigate the spectral response. The center of the spectrogram is used to minimize smile effects, and 50 rows are averaged to minimize noise. The spectrum, plotted together with known Fraunhofer lines, is shown in Figure 6.

The dips in the recorded spectrum were detected and compared with the Fraunhofer lines, presented in Table 4. The largest difference can be found at the oxygen A-band,

Table 4. Spectral shift, detected dips compared with known Fraunhofer lines.

Designated letter	**Fraunhofer wavelength [nm]**	**Recorded wavelength [nm]**	**Difference [nm]**
G[1]	430.8	429.2	1.6
e	438.4	438.3	0.1
d	486.1	487.0	-0.9
b_1	518.4	518.1	0.3
E_2	527.0	527.2	-0.2
D_1+D_2	589.3	590.6	-1.3
C	656.3	657.0	-0.7
B	686.7	688.7	-2.0
A	759.4	761.6	-2.2
Z	822.7	822.4	0.3

[1] Average value of G(Ca) 430.774 nm and G(Fe) 430.790 nm.

where the reference value is 759.37 nm and the recorded value 761.6 nm. The oxygen absorption lines come from absorption in the Earth's atmosphere, and varies as a function of height/pressure [10]. This leads to varying center wavelength of the bands, which can explain some of the variation seen here. There is no clear trend in the calculated differences, they are both positive and negative, and vary across the spectrum. This suggests that no clear spectral shift is detected. From the lines investigated, the Root Mean Square Error (RMSE) value is 1.21, which is quite large compared to the spectral calibration RMSE values reported in [2]. Spectral calibration coefficients of second order were applied to the data, as suggested in [11], which may introduce some inaccuracies. However, errors might also come from noise making it hard to detect the exact location of the absorption lines, specially for wavelengths with low SNR. Higher variation in the in-orbit data may also be caused by variations in the atmosphere, or from features of the Sahara Desert being present in the dataset.

4.4 Spatial shift

From pre-launch radiometric calibration (dataset 0b), shown in Figure 2, the edge of the slit is visible at the lower edge of the frame, and two horizontal stripes are visible at the top of the frame. In the Sahara full frame (dataset 2b) in Figure 4, the edge of the slit is again visible at the lower edge of the frame, while only one of the horizontal stripes are visible at the top. The exact spatial pixel location of the edge of the slit and the horizontal stripes are, however, not the same in the two frames.

The pixel location of both features (edge of slit and horizontal stripe) were investigated at spectral pixel 968 (corresponding to 600 nm), located approximately in the

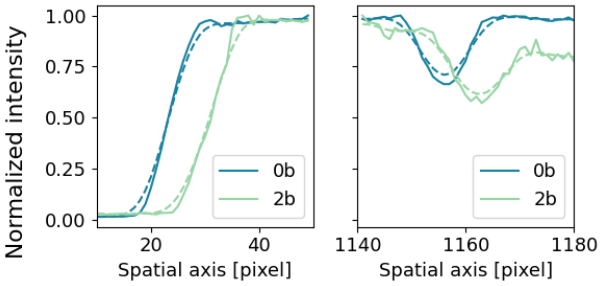

Fig. 7. Spatial shift. Edge of the spectrogram from bottom of the spectrogram (left), and horizontal line from the top of the spectrogram (right). Solid lines are before smoothing while dashed lines are smoothed.

center of the spectrogram. The lines (column in the spectrogram) were normalized by the maximum value, and smoothed, as presented in Figure 7. The solid lines show the lines before smoothing, while the dashed lines are smoothed. The areas around the features were isolated to better visualize the shifts.

The shift was calculated as the difference in pixel location of 50% of the normalized intensity for the edge of the slit (left in Figure 7). While for the horizontal stripe which appears as a dip in the plotted line (right in Figure 7) the shift was estimated as the change in pixel location of the minimum value of the dip. The shift was found to be 7 pixels for both the edge of the slit and the horizontal line. This was repeated for all wavelengths in the visible range (here 400 nm to 800 nm was used), and the average shift also found to be 7 pixels. Due to low signal at the edges of the spectrogram (below 400 nm and above 800 nm) the features and their shifts were disappearing in noise and therefore not detectable.

That a shift of 7 pixels is observed both in the upper and lower part of the spectrogram for all wavelengths suggests that either the slit (assuming the horizontal line is dust on the slit) has moved, or the camera sensor has moved relative to the optical train. The slit used is a COTS component, mounted inside a disc with 0.1 mm extra space within the mount. It is therefore likely that the shift observed is caused by the slit having moved inside its casing during launch.

4.5 Destriping

Once the consistency of the sensor calibrations has been evaluated, strategies for data analysis which can accommodate the shifts in the sensor must be found. The correction must be powerful enough to mitigate the shifts in the calibration, but must also be simple enough to avoid inducing any new errors into the data. Any new set of radiometric calibration coefficients which were deduced by the Sahara images would be impaired by the spatial features in those images, so instead a simple correction to the

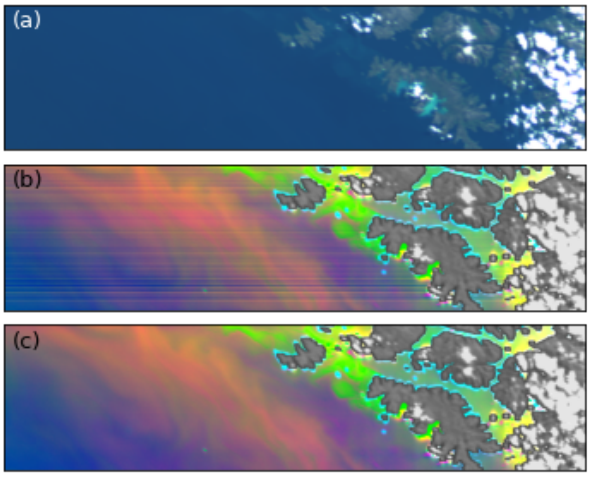

Fig. 8. (a) A HYPSO-1 image near Sørøya, Norway (dataset 3a). (b) The first three principal components of the water in the image represented in the green, blue, and red color channels, without destriping. (c) The same three components after destriping.

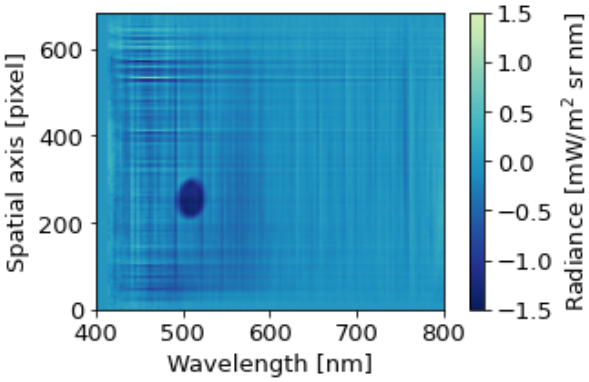

Fig. 9. Additive across-track correction calculated from radiance over water.

ground calibration is tested.

It is common for stripes to appear in hyperspectral images, due to a number of issues including hot pixels and spectral calibration shifts [12]. Although these stripes are typically quite small in magnitude relative to the entire spectral signature, they can interfere with the analysis of small signals, for example changes to the constituent particles in water. Because of the shifts in the calibration noted above as well as hot pixels, these stripes are present in the hyperspectral data collected by HYPSO-1 (Figure 8a and Figure 8b).

To mitigate the effect of these stripes, their magnitude was evaluated and an additive correction developed to apply to the data cube. Although the stripes potentially come from both multiplicative and additive factors (changes in radiometric calibration and hot pixels, respectively), only

water pixels, which have a fairly consistent spectrum, are selected for the analysis so that both effects can be approximated by an additive correction. The change in intensity between each pair of neighboring cross-track radiance pixels, $\Delta I(\lambda)$ is calculated. Then, the median of each along-track column of $\Delta I(\lambda)$ is selected as the correction. The $\overline{\Delta I(\lambda)}$ are then integrated cross-track to generate the additive correction for each position on the spatial axis, for each wavelength, shown in Figure 9.

The similarity of the features in the additive correction and in the Sahara frame, including the smudge and horizontal lines (Figure 5), suggests that the correction compensates for real artifacts in the data. Moreover, after the correction is applied to the HYSPO-1 scene (Figure 8c), horizontal stripes are no longer visible in the the first few principal components.

5. Conclusions

Overall, the hyperspectral data from HYPSO-1 appears as expected, except for the new smudge discovered at spatial pixel 700 and spectral pixel 700 (wavelength 500 nm), and the spatial shift of 7 pixels. Corrections for the spatial shift could possibly be mitigated by shifting the calibration coefficients (which might affect the accuracy of the calibration, this must be assessed during correction), while the smudge should be characterized by performing radiometric calibration in-orbit. Adjusting the radiometric calibration in-orbit could also correct the spatial shift. No spectral shift was detected, but monitoring the spectral position of Fraunhofer lines or the oxygen A-band can be useful to ensure no spectral drift in-orbit.

The dark images show that most values are at around 8 counts, which is the estimated background value from pre-launch calibration. Higher background counts are detected when longer exposure times are used, which can be due to higher temperature increase induced with longer exposure times. When investigating hot pixels, some are recorded, and the higher numbers again found for the data captured with longer exposure times. Hot pixels in different datasets are, however, not located at the same pixels, which makes a general correction harder to provide.

A simple, additive algorithm for destriping hyperspectral images is tested on an exemplary data cube. Because the generated correction shows features similar to those found in the radiometric analysis of the Sahara data, it is likely that further in-flight calibrations can be used to develop a more comprehensive correction to the pre-flight calibrations, so that a standard destriping procedure can be developed. Moreover, the success of the destriping is readily visible in the first few principal components of the water pixels in an image, indicating that the further development of these corrections will greatly enhance the capacity of HYPSO-1 to contribute to water monitoring programs.

Acknowledgements

This work was supported by the Research Council of Norway through the Centre of Excellence funding scheme (NTNU AMOS, grant no. 223254) and the IKTPLUSS project MASSIVE (grant no. 270959), the Norwegian Space Agency and the European Space Agency through PRODEX (no. 4000132515), and research leading to these results has received funding from the NO Grants 2014 – 2021, under Project ELO-Hyp, contract no. 24/2020. The authors would also like to thank the full HYPSO-1 team for all the work done to accomplish a successful launch, and the operational team for acquiring data from the satellite.

References

[1] M. E. Grøtte et al. “Ocean Color Hyperspectral Remote Sensing With High Resolution and Low Latency—The HYPSO-1 CubeSat Mission”. In: *IEEE Transactions on Geoscience and Remote Sensing* 60 (2022), pp. 1–19. DOI: 10.1109/TGRS.2021.3080175.

[2] M. B. Henriksen et al. “Pre-Launch Calibration of the HYPSO-1 Cubesat Hyperspectral Imager”. In: *IEEE Aerospace Conference*. 2022. ISBN: 9781665437608.

[3] E. F. Prentice et al. “Pre-Launch Assembly, Integration, and Testing Strategy of a Hyperspectral Imaging CubeSat, HYPSO-1”. [accepted]. 2022.

[4] E. F. Prentice et al. “Characterizing Spectral Response in Thermal Environments, the HYPSO-1 Hyperspectral Imager”. In: *IEEE Aerospace Conference*. 2022.

[5] M. B. Henriksen et al. “Do-it-yourself VIS/NIR pushbroom hyperspectral imager with C-mount optics”. In: *Optics Continuum* 1.2 (2022), p. 427. ISSN: 25787519. DOI: 10.1364/optcon.450693.

[6] E. F. Prentice et al. “Design of a hyperspectral imager using COTS optics for small satellite applications”. In: *Proc. SPIE 11852, International Conference on Space Optics – ICSO 2020, 1185258*. 2021.

[7] F. Weiler et al. “Characterization of dark current signal measurements of the ACCDs used on board the Aeolus satellite”. In: *Atmospheric Measurement Techniques* 14.7 (2021), pp. 5153–5177. ISSN: 1867-8548. DOI: 10.5194/amt-14-5153-2021.

[8] P. Du Buisson et al. “In-flight spectral calibration of the oxygen A-band channel of MERIS”. In: *International Journal of Remote Sensing* 24.5 (2003), pp. 1177–1182. ISSN: 01431161. DOI: 10.1080/0143116021000031809.

[9] D. A. Newnham and J. Ballard. “Visible absorption cross sections and integrated absorption intensities of molecular oxygen (O2 and O4)”. In: *Journal of Geophysical Research Atmospheres* 103.D22 (1998), pp. 28801–28815. ISSN: 01480227. DOI: 10.1029/98jd02799.

[10] D. Q. Wark and D. M. Mercer. “Absorption in the Atmosphere by the Oxygen "A" Band”. en. In: *Applied Optics* 4.7 (1965), p. 839. ISSN: 0003-6935, 1539-4522. DOI: 10.1364/AO.4.000839.

[11] M. B. Henriksen, F. Sigernes, and T. A. Johansen. “A Closer Look at a Spectrographic Wavelength Calibration”. In: *12th Workshop on Hyperspectral Image and Signal Processing, Evolution in Remote Sensing (WHISPERS)*. [accepted]. 2022.

[12] J. D. Ortiz et al. “Evaluating visible derivative spectroscopy by varimax-rotated, principal component analysis of aerial hyperspectral images from the western basin of Lake Erie”. In: *Journal of Great Lakes Research* 45.3 (2019), pp. 522–535.